Stoch Environ Res Risk Assess (2013) 27:1155–1170
DOI 10.1007/s00477-012-0651-4

ORIGINAL PAPER

Power spectral characteristics of drought indices in the Ebro river basin at different temporal scales

L. Telesca · S. M. Vicente-Serrano · J. I. López-Moreno

Published online: 7 October 2012

Abstract A deep spectral investigation of the monthly time series of Standardized Precipitation Index (SPI) and Standardized Precipitation Evapotranspiration Index (SPEI) in 45 meteorological stations in the Ebro basin (Spain) from 1950 to 2006 for timescales ranging from 1 to 48 months was performed. In order to summarize the results for the whole basin, the spectral analysis was also carried out on the four principal components of SPI and SPEI. Results confirm that SPI and SPEI presents very similar spectral characteristics. At the shorter time scales, the signal of SPI and SPEI is characterized by purely random temporal fluctuations. The longer time scales tend to feature the signal as a smoothly varying time series or persistent, mostly due to the aggregated nature of the indices calculation. The comparative analysis of the spectral properties of the drought indices for all the 45 sites in the Ebro basin lead to the identification of global or regional effects discriminated by local effects. It was found that some periodical signals are common to almost all the sites, while others where only identified in specific meteorological stations.

Keywords Standardized Precipitation Index · Standardized Precipitation Evapotranspiration Index · Power spectrum · Principal component analysis

L. Telesca (✉)
National Research Council, Institute of Methodologies for Environmental Analysis, C.da S.Loja, 85050 Tito, PZ, Italy
e-mail: luciano.telesca@imaa.cnr.it

S. M. Vicente-Serrano · J. I. López-Moreno
Instituto Pirenaico de Ecología, CSIC, Campus de Aula Dei. Avda. Montañana 1005, 50.059 Zaragoza, Spain

1 Introduction

Droughts are one of the main natural hazards that affect the Mediterranean region. In this area droughts have severe consequences for agriculture and natural vegetation (Lázaro et al. 2001; Reichstein et al. 2002; Iglesias et al. 2003), increasing the frequency of fires (Colombaroli et al. 2007; Pausas 2004) and significantly reducing water availability for urban and tourist consumption (Morales et al. 2000). The identification of drought events is a difficult task since we identify a drought by its effects at different levels, but there is not a physical variable we can measure to quantify droughts. In addition it is very difficult to clearly identify their beginning, the duration and quantify its magnitude in both, time and space (Wilhite 1993). The impact of a given drought on different natural or socioeconomic frames will depend largely on the temporal persistence of the drought conditions, as the different subsystems of the water cycle (i.e. soil moisture, streamflows, snowpack, aquifers or water stored in lakes or artificial reservoirs) have a different time of response to antecedent climatic conditions (Vicente-Serrano et al. 2011). For this reason, drought is considered as a multi-scalar phenomenon (McKee et al. 1993). Such multiscalar character and the difficulties to delimit droughts in time and space have promoted to invest large efforts on the development and improvement of climatic drought indices which permit to assess objectively the magnitude and extent of a drought event from climatic information (see reviews in Heim 2002; Keyantash and Dracup 2002; Mishra and Singa 2010; Sivakumar et al. 2010).

In the last years, the Standardized Precipitation Index (SPI, McKee et al. 1993) has been widely used and highlighted for a number of advantages over other indices (Guttman 1998; Keyantash and Dracup 2002). It needs only precipitation monthly data for its computation, it

employs a moving average that facilitates spatial comparability (Guttman 1998), it is valid for any season, and the results are not affected by topography (Lana et al. 2001). In addition, the length of the precipitation record and the period used for calculation do not significantly affect the final calculation of the SPI (Wu et al. 2005). Thus, given its substantial advantages in quantifying and monitoring droughts, the SPI has been accepted by the World Meteorological Organization as the reference drought index. In the "Lincoln Declaration on Drought Indices," 54 experts from all regions of the world agreed on the use of a universal meteorological drought index for more effective drought monitoring and climate risk management. They made the significant consensus agreement that the Standardized Precipitation Index (SPI) should be used by national meteorological and hydrological services worldwide to characterize meteorological droughts (Hayes et al. 2011). More recently, Vicente-Serrano et al. (2010a, b) developed the Standardized Precipitation and Evapotranspiration Index (SPEI), which is computed from the monthly climatic water balance (precipitation minus potential evapotranspiration) instead of using only precipitation. In this manner, the effect of evapotranspiration on certain drought events is now possible to be included in the computation of the drought duration and magnitude maintaining the same capability of SPI to monitor drought at different time scales. The SPEI has advantages over previous indicators because it combines the sensitivity of the Palmer Drought Severity Index to changes in evaporation demand (caused by temperature fluctuations and trends), simplicity of calculation, and the multi-temporal nature of the SPI.

Many studies have analysed the temporal evolution of drought indices (i.e. SPI and SPEI) at different time scales for different regions (e.g., Lloyd-Hughes and Saunders 2002; Vicente-Serrano 2006a, b; Bari Abarghouei et al. 2011; Du et al. 2012; Moreira et al. 2012), or they have related the drought anomalies with the fluctuations of water resources availability in different subsystems of the water cycle or ecological indicators (Lorenzo-Lacruz et al. 2010; Vicente-Serrano 2007; Quiring and Ganesh 2010; Pasho et al. 2011). However, much lesser studies have analyzed the temporal structure of these indices in order to identify scaling behavior and periodicities in the temporal series of the drought indices, as it was done by Santos et al. (2010) using the SPI index in Portugal, who demonstrated the existence of different periodicities for different time scales and geographical sectors of the country.

In this study, we analyze the power spectral characteristics of the SPI and SPEI index in the Ebro river basin. This is a Mediterranean river basin affected by periodic intense droughts (Vicente-Serrano 2006b; Vicente-Serrano and Cuadrat-Prats 2007; Vicente-Serrano and López-Moreno 2006) and characterized by a marked contrast in climatic conditions as a consequence of the complex topography and the geographical location between the Atlantic Ocean and the Mediterranean sea (López-Moreno et al. 2011). The main purpose of the study is to assess whether the spectral characteristics of SPI and SPEI differ as a consequence of the inclusion of potential evapotranspiration in the computation of the later. Moreover, the conducted analyses will allow to test how spectral properties of SPI and SPEI changes with different time scales, and to identify geographical differences in the temporal evolution and spectral structure of SPI and SPEI indices.

2 Study area

The Ebro basin has an extent of about 83,000 km^2 in the northeast of Spain and has very contrasting relief. The main unit is the Ebro Valley, which is a depression surrounded by high mountain ranges including the Cantabrian Range and the Pyrenees to the north, the Iberian mountains to the south, and the Coastal Range to the east. The heterogeneous topography, contrasting influences of Atlantic and Mediterranean conditions, and the influence of various large scale atmospheric patterns (Vicente-Serrano and López-Moreno 2006) generate a complex spatial distribution of climate parameters. Large variations in precipitation and evapotranspiration occur throughout the region (Vicente-Serrano et al. 2010a, b), and annual precipitation varies from 307 to 2,451 mm yr^{-1}. Average annual temperature varies from 0.8 to 16.2 °C.

The humid conditions in the mountainous areas are in contrast to the dry climate of the lowlands, emphasizing the importance of hydrology and water resources throughout the study region. Moreover it exits a trancsition of oceanic climate to Mediterranean conditions from west to east (López-Moreno et al. 2011). The relative abundance of water in the area led to the construction of numerous dams to regulate the main rivers, which markedly altered river regimes and reduced flood occurrence. Most of the dams were built between the 1950s and the 1980s, leading to an increase in storage capacity from 500 to 3,000 hm^3; they have introduced noticeable alterations of river regimes and flood occurrence (López-Moreno and García-Ruiz 2007).

3 Data

Drought indices were calculated in 45 observatories located within the Ebro basin or in its immediate surroundings. These observatories recorded simultaneously temperature and precipitation data since 1950–2006. Definitive climatic series were obtained from raw data processing including

stations reconstruction, gap filling, quality control and homogenization testing with independent reference series (see Vicente-Serrano et al. 2010a, b; El Kenawy et al. in press).

The SPI calculation is based on precipitation records summarised on different time scales. The total precipitation $X_{i,j}^k$ in a given month j and year i depends on the time scale chosen, k. For example, the 12-month SPI for one month in a particular year i with a 12-month time scale is calculated according the following formulae (Paulo et al. 2003):

$$X_{i,j}^k = \sum_{l=13-k+j}^{12} w_{i-1,l} + \sum_{l=1}^{j} w_{i,l}, \quad \text{if } j < ; k, \tag{1}$$

and

$$X_{i,j}^k = \sum_{l=j-k+1}^{j} w_{i,l}, \quad \text{if } j \geq k \tag{2}$$

where $w_{i,1}$ is precipitation in the lst month of year i [mm].

Among different models, the Pearson III shows an enhanced adaptability to precipitation series at different time scales (Guttman 1999; Vicente-Serrano 2006b). In our study, Pearson III distribution was chosen to calculate SPI for time scales from 1 to 12 months.

According Pearson III distribution, the probability distribution function of x is given by:

$$F(x) = \frac{1}{\alpha\Gamma(\beta)} \int_{\gamma}^{x} \left(\frac{x-\gamma}{\alpha}\right)^{\beta-1} e^{-\left(\frac{x-\gamma}{\alpha}\right)} \tag{3}$$

where α, β and γ are the shape, scale and origin parameters, respectively, for precipitation values $x > 0$; and $\Gamma(\beta)$ is the Gamma function of β.

Parameters of the Pearson III distribution were obtained according to the L-moment approach, following an unbiased estimator (Hosking 1990).

Pearson III distribution is not defined for $x = 0$, which is a drawback as precipitation series may include months in which there is no precipitation. With this in mind, an adapted statistic $H(x)$ can be calculated using the following formula (Edwards and McKee 1997):

$$H(x) = q + (1-q)F(x) \tag{4}$$

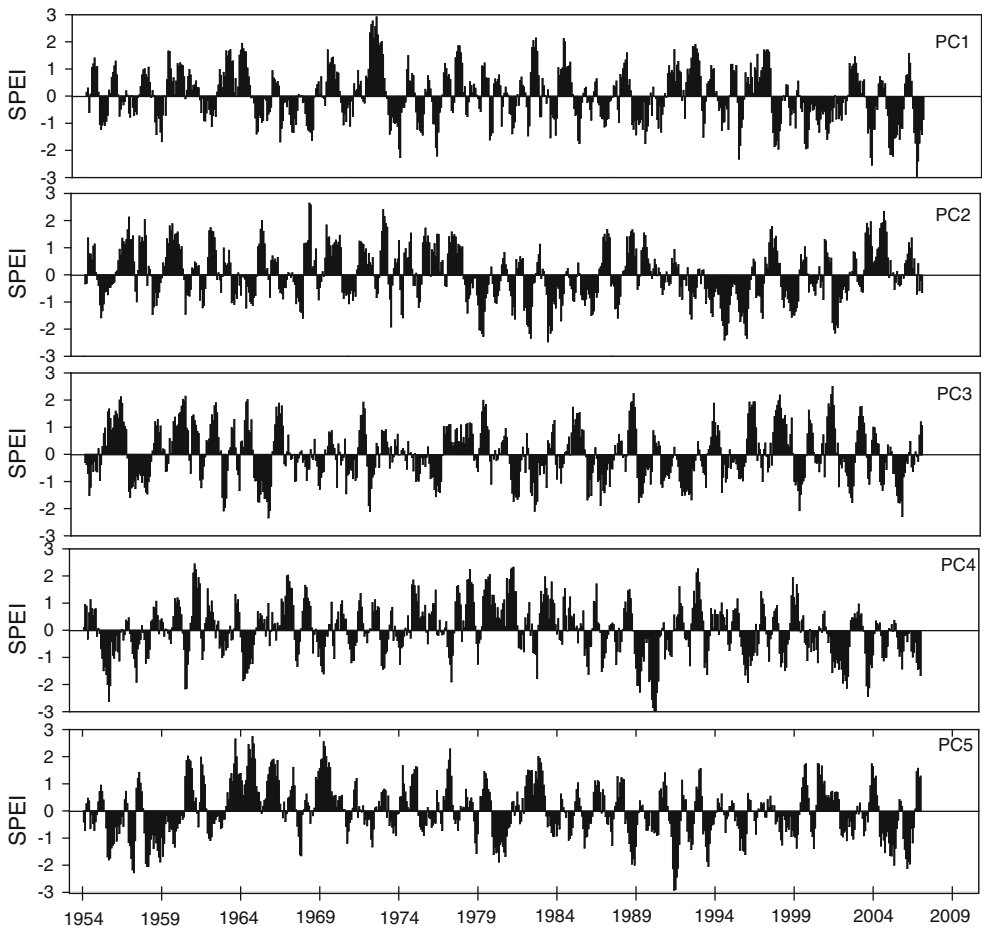

Fig. 1 The five principal components which summarize more than a 70 % of the variance from the 45 SPEI series at a time scale of 6 months

where q is the probability of zero precipitation. q can be calculated simply as m/n, where n is the total number of months and m is the number of months with no precipitation.

After calculating $H(x)$, the mean is standardised as 0 and standard deviation as 1. This standardised variable is interchangeable with the SPI, and is commensurable with other SPI values over time and space. An SPI of 0 indicates precipitation corresponding to 50 % of accumulated probability according to Pearson III distribution. To transform $H(x)$ and obtain normalised SPIs, the classical approach formulated by Abramowitz and Stegun (1965) was used.

The SPEI is based on a monthly climatic water balance (precipitation minus potential evapotranspiration) adjusted using a three-parameter log-logistic distribution to take into account common negative values (Vicente-Serrano et al. 2010a, b). The SPEI was calculated according Thorthwaite's equation. The probability distribution function of the series according to the Log-logistic distribution is given by:

$$F(x) = \left[1 + \left(\frac{\alpha}{x - \gamma}\right)^{\beta}\right]^{-1}. \quad (5)$$

The L-moment procedure was used to obtain the parameters of the Pearson III distribution, following Singh and Guo (1993). With $F(x)$ the SPEI is easily obtained as the standardized values of $F(x)$, following again the classical approximation of Abramowitz and Stegun (1965). Details of the calculation of the SPI and the SPEI can be found in López-Moreno and Vicente-Serrano (2008) and Vicente-Serrano et al. (2010a, b).

4 Methods

4.1 The principal component analysis

The Principal Component Analysis (PCA) is a widely used procedure of identifying patterns in climatic and hydrological data (Smith 2002). The PCA permits to reduce the original dimensionality of the data thanks to the extraction of a some uncorrelated variables which explain a large portion of the total variance. As Santos et al. (2010) did for SPI series of Portugal, we performed individual PCA analysis for SPI and SPEI series at times scales of 1, 3, 6, 12 and 24 months, in order to assess their spatial and temporal patterns. To guarantee the stationarity of the time series, before calculating the principal components of the SPI and SPEI series on different time scales, we detrended them using linear adjustments and residual values.

We performed the PCA in S-mode (correlation between time series) to obtain the general temporal patterns of SPI and SPEI at different time scales. This mode provides loading values corresponding to each pattern, which can then be represented spatially. For the PCA, we used a correlation matrix. The number of components was chosen so that the total explained variance was at least 70 %. Finally, the components were rotated to redistribute the final explained variance and to obtain more stable and physically robust patterns (Richman 1986). For this purpose, we used the Varimax rotation, which provides clearer and physically explainable patterns (Jolliffe 1990). As an example, Fig. 1 shows the five principal components which summarize more than 70 % of the variance from the 45 SPEI series at the time scale of 6 months. Within the study area different patterns can be found in the temporal evolution of SPEI, characterized by phases of positive and negative magnitude and by the occurrence of dry and wet periods. Power spectral density analyses were further applied to each component for SPI and SPEI at the considered time scales (1, 3, 6, 12, 24 months) to assess the scaling properties of the different drought indices across the study area.

4.2 Power spectral density

The power spectrum is a method that allows identifying mainly relatively strong oscillations, given by frequency peaks with relatively high amplitude, and scaling behaviour, indicated by a power-law form of the power spectrum at certain frequency bands. An oscillation indicates that the process is modulated with a characteristic frequency, given by the inverse of the period of that oscillation; a scaling behaviour indicates that there are not typical characteristic

Table 1 PCA results. Cumulative explained variance of the PCA applied to SPI and SPEI temporal series at different scales

Temporal scale	SPI: explained variance (%)					SPEI: explained variance (%)				
	PC1	PC2	PC3	PC4	PC5	PC1	PC2	PC3	PC4	PC5
1 month	22	37	51	63	72	18	35	49	66	72
3 months	21	36	50	62	72	23	41	57	71	77
6 months	43	57	64	69	72	22	41	57	71	75
12 months	18	33	46	57	68	20	35	48	59	68
24 months	36	50	59	65	71	19	38	51	61	69

Fig. 2 Distribution of the meteorological stations that exhibited a higher correlation with the different principal components (PCs)

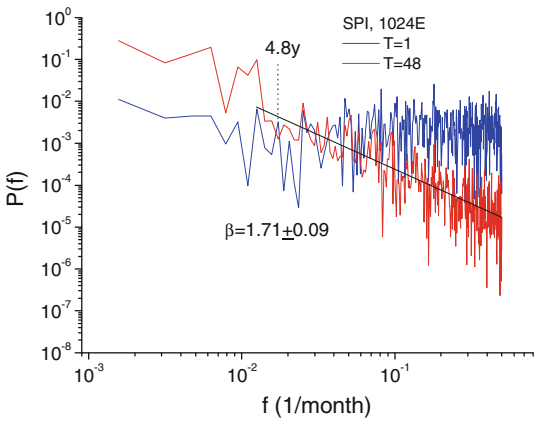

Fig. 3 Comparison between the power spectra of SPI_1 and SPI_{48} for the site 1024E

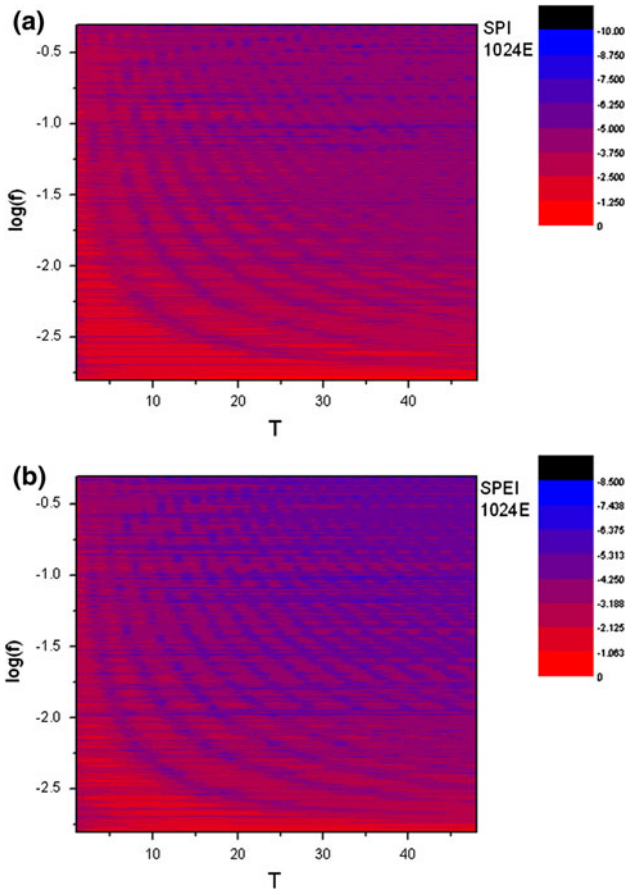

Fig. 5 Bi-dimensional pattern of the logarithm of the power spectra of the SPI (**a**) and SPEI (**b**) varying the logarithm of the frequency f (on the *y*-axis) and the timescale T (on the *x*-axis) for the site 1024E. The *color bar* indicates the logarithm of the intensity of the power spectrum. (Color figure online)

frequencies, contrarily to what happens, for instance, for exponential distributions. The strength of an oscillation is quantified by the amplitude of the corresponding frequency peak; while the strength of the scaling is quantified by the exponent of the power-law that fits the spectrum in a certain frequency band (the slope of the line fitting in a least-square sense the power spectrum plotted in log–log scales). The scaling is also typical of memory phenomena and indicates the presence of correlation structures in the process. As opposite, the white noise does not present dominant oscillations nor scaling behaviour (it is flat for any frequency band); thus it can be used to test the significance of both the features in a power spectrum.

5 Analisys

5.1 Principal component analysis: spatial variability of droughts

Table 1 summarizes the results of the Principal Component Analyses (PCA) for SPI and SPEI series at times scales of 1, 3, 6, 12 and 24 months, as an example. In almost all cases 5 components are enough to explain at least a 70 % of the variance. Figure 2 shows the distribution of the meteorological stations that exhibited the maximum correlation with any of the different principal components

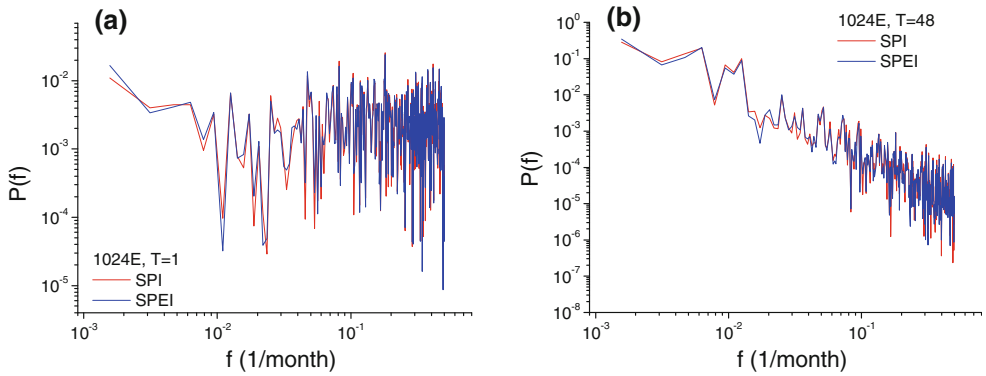

Fig. 4 Comparison between the power spectra of SPI_1 and $SPEI_1$ (**a**) and that between the power spectrum of SPI_{48} and $SPEI_{48}$ (**b**)

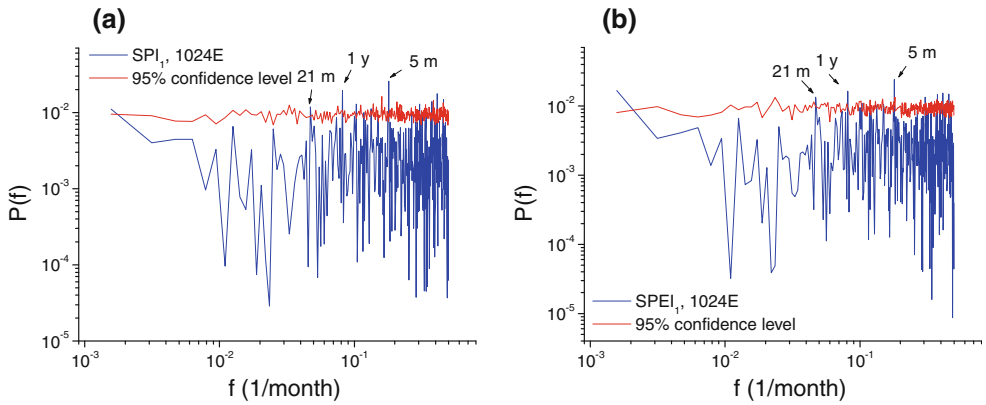

Fig. 6 Power spectrum of the SPI_1 (**a**) and $SPEI_1$ (**b**) along with their 95 % confidence curve (*red line*) for the site 1024E. (Color figure online)

(PCs). In general, there is a spatial coherence in the distribution of stations associated to each PC. In some cases, all stations have exhibited a maximum correlation with two or three component identified in the PCA analysis (i.e. at 1 month time scale). In other cases, SPEI and SPI series have exhibited a more contrasted spatial variability, and different groups of stations are related to the 5 different PCs. In general, there is a good association in the spatial differences identified for SPI and SPEI indices. Only for SPI at 3-months time scale shows a larger spatial variability in the series, and the opposite occurs for SPEI at 12 months, when it exhibits a higher variability than SPI.

5.2 Spectral analysis of SPI and SPEI time series

We calculated the power spectra of the SPI and SPEI time series for each of the investigated sites by using the periodogram method. As an example, we show the spectral analysis performed for the site 1024E. Figure 3 shows the comparison between the power spectra of SPI_1 and SPI_{48} for the site 1024E, where the subscript indicates the time scale as defined in Sect. 3. Both the spectra show a quite flat behaviour in the very low frequency band up to approximately the frequency $f_0 \approx 0.017$ month^{-1} (corresponding to a period of approximately 4.8 years), for higher frequencies the power spectrum of SPI_1 keeps on being approximately flat, while that of SPI_{48} scales with the frequency with a decreasing power-law shape (linear in log–log scales) with scaling exponent $\beta \approx 1.7$. The SPI time series for the intermediate timescales are characterized by a shape of the power spectra approximately intermediate between those of SPI_1 and SPI_{48}. The power spectrum of SPEI at the site 1024E has a very similar form as that of the SPI; Fig. 4 shows the comparison between the power spectra of SPI_1 and $SPEI_1$ (Fig. 4a) and that between the power spectrum of SPI_{48} and $SPEI_{48}$ (Fig. 4b). Figure 5 shows the bi-dimensional pattern of the logarithm of the power spectra $P(f)$ of the SPI (Fig. 5a) and SPEI (Fig. 5b) varying the logarithm of the frequency f (on the y-axis) and the timescale T (on the x-axis) for the site 1024E. It can be observed that for the lower timescales the power spectrum is distributed on the frequency more homogenously than for higher timescales; in fact, for the higher timescales, the most of the power is concentrated in the lower frequency bands.

By using the power spectrum, the signal is decomposed in series of cycles (represented by frequency lines), whose power is indicated by the amplitude (given by the height of the lines); the larger the amplitude, more powerful the cycle, more intense the modulating effect of such cycle on the whole series. The identification of strong cycles or oscillations in a signal is crucial for the identification of possible external factors that could be responsible of such oscillatory behavior of the process. In order to identify significant cycles in the power spectra of the SPI and SPEI time series, we used the shuffling procedure. By this method, we generated simulated series having the same statistical features of the original ones (the same probability density function) but characterized by white-noise spectral features (approximately flat power spectrum). Thus, our aim was to check the significance of the cycles against the white noise hypothesis. The original time series was shuffled one thousand times; the shuffling procedure destroys all the inner time structures and make the time series a realization of white noise (Telesca 2010). For each shuffle, the power spectrum was calculated. Then, to test the significance of a particular frequency, the 95-th percentile of the distribution of the values of the shuffle power spectra was calculated, giving the 95 % confidence level for that frequency; therefore, if the corresponding value of the power spectrum of the original time series is above the 95 % confidence level, that frequency is significant with 95 % confidence. Figure 6 shows the power spectrum of the SPI_1 (Fig. 6a) and $SPEI_1$ (Fig. 6b) along with their 95 % confidence curve (red line) for the site 1024E. The power spectrum of the SPI_1 is approximately flat, mostly

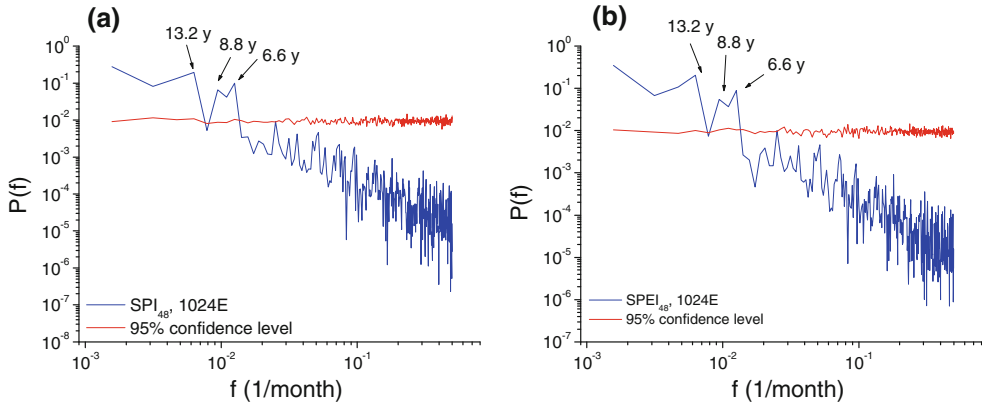

Fig. 7 Power spectrum of the SPI_{48} (**a**) and $SPEI_{48}$ (**b**) along with their 95 % confidence curve (*red line*): both indices shows the same significant cycles at 13.2, 8.8 and 6.6 years. (Color figure online)

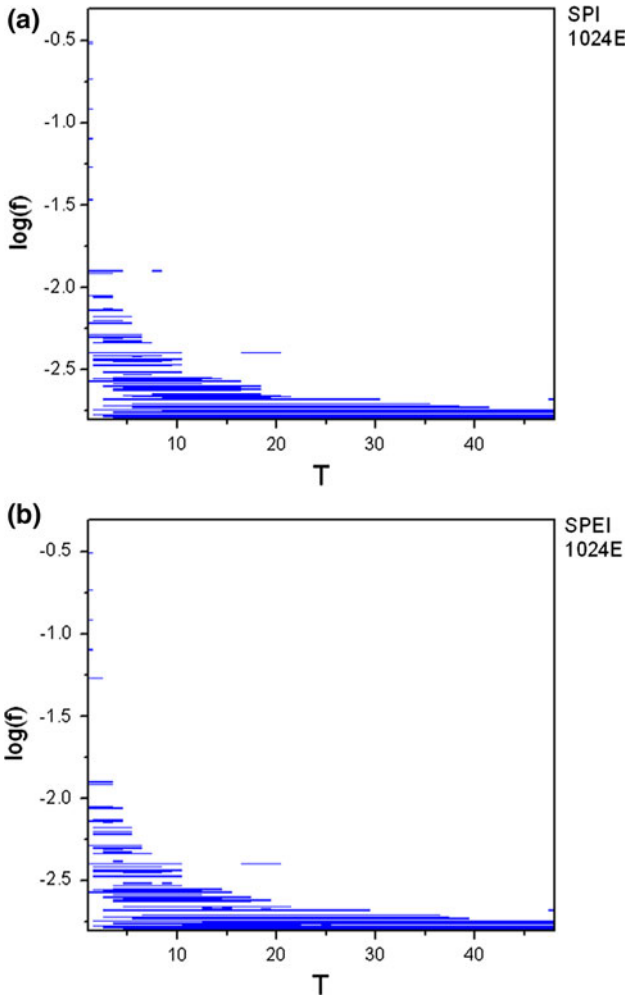

Fig. 8 The 95 % significant cycles of SPI (**a**) and SPEI (**b**) for the site 1024E. The variable T is measured in months

below the 95 % confidence curve, with few frequency peaks slightly above the 95 % confidence curve, in particular, the 21-month, 1-year and 5-month cycles; therefore, we can deduce that the SPI_1 time series of the site 1024E (San Sebastian, in the Atlantic Ocean coast) is mostly a realization of a white noise process, but very weakly modulated by the three cycles at 21 months, 1 year and 5 months. $SPEI_1$ shows almost identical spectral characteristics; it is mainly characterized by purely random time variability, but very weakly modulated by the three cycles. Figure 7 shows the power spectrum of the SPI_{48} (Fig. 7a) and $SPEI_{48}$ (Fig. 7b) along with their 95 % confidence curve (red line): both indices shows the same significant cycles at 13.2, 8.8 and 6.6 years.

Figure 8 shows the 95 % significant cycles of SPI (Fig. 8a) and SPEI (Fig. 8b) for the site 1024E, versus the timescale *T*, which ranges from 1 to 48 months; any blue cell represents a significant cycle whose amplitude is above the 95 % confidence level. From these results we can observe that cycles with the lower frequencies are almost common for all the timescales *T*, while cycles with higher frequency are significant only for the time series with lower timescale *T*. Moreover, the time series corresponding to lower timescales present more significant cycles than the time series corresponding to higher timescales.

It is worth analyzing if a cycle is significant for many sites or only for few sites: in the first case, the cycle could be linked to some global effects that influence the hydrology of the whole watershed; in the second case, the cycle could describe local effects that are linked with the hydrology of the particular site. Figure 9 shows, as an example, the distribution of the significant cycles/site for the 3-month, 12-month and 24-month timescale for the SPI and the SPEI time series. Concerning the SPI_3 (Fig. 9a) three significant cycles (8 months, 1.6 years and 3.1 years) are present in the most of the sites, other cycles (5.3 years, 4.1 years, 2.6 years, 1 year) are present in approximately 2/3 of the sites, others are common only to few sites. Similar observations can be done for the $SPEI_3$ (Fig. 9b). For the $SPI_{12,24}$ and $SPEI_{12,24}$ (Figs. 9c–f)we can see that the 3.1-year,

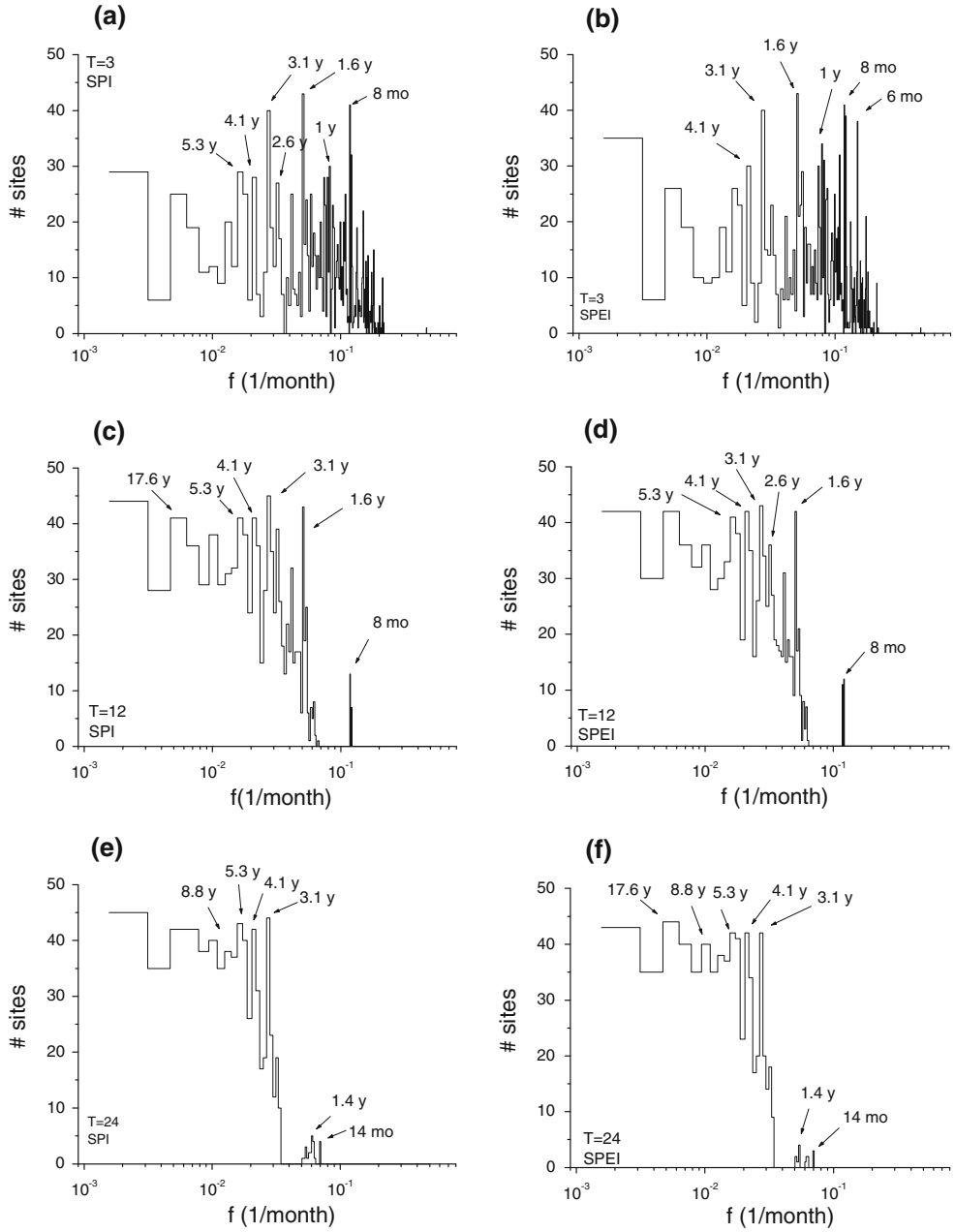

Fig. 9 Distribution of the significant cycles for the 3-month, 12-month and 24-month timescale for the SPI (**a**–**f**) and the SPEI (**g**–**l**) time series

4.1-year, the 5.3-year, the 8.8-year and the 17.6-year cycles are common to most of the sites, while the 8-month and 1.4-year cycle are common to few sites. The 3.1-year, 4.1-year and 5.3-year cycles are evidenced at any timescale and in the most of the sites, therefore, such cycles would be indicative of global effects (i.e. cycles in atmospheric circulation patterns) that could influence the whole watershed.

Figure 10 shows the number of the sites in which identical significant cycles of SPI and SPEI exist for each timescale: as commented on the results regarding the particular cases shown in Fig. 9, we observe that the lower frequency (higher period) cycles are common to the most of the timescales in the most of the measuring sites, while the higher frequency (lower period) cycles are significant for few sites and only for the lower timescales.

5.3 Spectral analysis of the main components of PCA

The periodogram method was used to analyse the spectral properties of the SPI and SPEI patterns obtained by means of the PCA for the Ebro watershed. Figures 11, 12, 13, 14, 15, 16, 17, 18 show the power spectral density of the first four

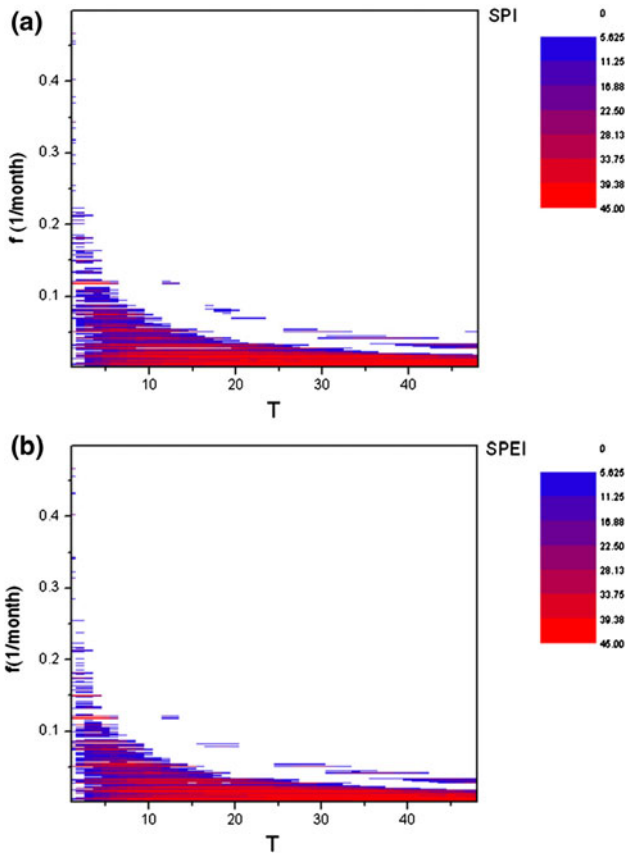

Fig. 10 Number of the sites in which identical significant cycles of SPI and SPEI exist for each timescale. The *color bar* indicates the number of sites. (Color figure online)

PCA components of the SPI and SPEI for the timescales $T = 1, 3, 6$ and 12 months. In each plot the 95 % confidence curve is also plotted (red). Thus, the significant cycles are indicated by the frequency peaks above the confidence curve. In some cases a peak corresponding to very low frequency (indicated by a blue arrow in the plots) is more prominent than the other cycles; anyway, it is not so intense to hide the other cycles, which are clearly visible. The spectral analysis of the first four components F1–F4 of SPI_1 show the predominance of high frequency (low period) cycles (at 3–6 months in F1, F3 and F4), the yearly cycle (in F2) and the 2.6-year oscillation (in F3) (Fig. 11). The spectral analysis of the PCA components of SPI_3 reveals the predominance of the cycle with period 1.6 years (in F1), 1.1 years (in F2) and 2.6 years (in F3), while regarding F4 there is a certain richness in the spectral behaviour with the presence of several significant cycles with periods ranging between 6.6 years and 6 months, with the most intense cycle at around 10 months (Fig. 12). Regarding SPI_6, single cycles are predominant in each PCA component with periods ranging between 1.6 years and 3 years (Fig. 13). Similar findings can be observed in the power spectra of the PCA components of SPI_{12}, with the evidence of the 4.8-year cycle (in F1), 2.6-years (in F2), 13.2-years (in F3) and 4.1-years (in F4) (Fig. 14). The power spectral densities of the PCA components for the $SPEI_{1,3,6,12}$ are approximately similar to those of the $SPI_{1,3,6,12}$, with only very slight differences in the intensity and period of the cycles (Figs. 15, 16, 17, 18).

6 Discussion

In this paper we performed the analysis of the time fluctuations of the monthly SPI and SPEI of 45 different sites widespread in the Ebro Basin (Spain). The analysis highlighted the following features:

(i) *Spectral similarity between SPI and SPEI*. The spectral characteristics of both indices are quasi identical in terms of power spectrum shape (from approximately flat at small timescales to power-law at high timescales), and in terms of periodical signals detected. Such strong similarity in the dynamical behavior is indicative that both indices can be used for drought analysis.

(ii) *Shape of the power spectrum*. The shape of the power spectrum reveals the type of the temporal fluctuations inherent in the time series: an approximately flat power spectrum indicates that the signal is characterized by purely random temporal fluctuations, which should prevent to use such signal for predictions that could be unfeasible due to its inherently memoryless nature. Such behavior was evidenced for the SPI and SPEI corresponding to the low timescales. If the power spectrum behaves as a power-law, then the process is characterized by memory phenomena and correlated structures; if it behaves, in particular, as a decreasing power-law, then the signal is governed by positive feedbacks, and this means that the signal is characterized by an inner dynamics that tends to reinforce the variations so that if the signal increases (decreases), it will keep on increasing (decreasing), this featuring the signal as a smoothly varying time series or persistent. On the contrary, an antipersistent signal is characterized by negative feedback mechanisms that tend to annihilate the signal variations, so that if the signal increases (decreases), it will tend to decrease (increase). This behavior mainly characterizes the SPI and SPEI corresponding to the longer timescales, which could be more efficiently used for drought forecasting investigations and predictability of dry/wet ranges. However, it should be observed that the power-law found in both indices corresponding to the longer timescales should not be interpreted as an indicator of the presence of inner correlated phenomena in the hydrological process, but rather as an effect of procedure of calculating the SPI (McKee et al. 1993), which accumulates

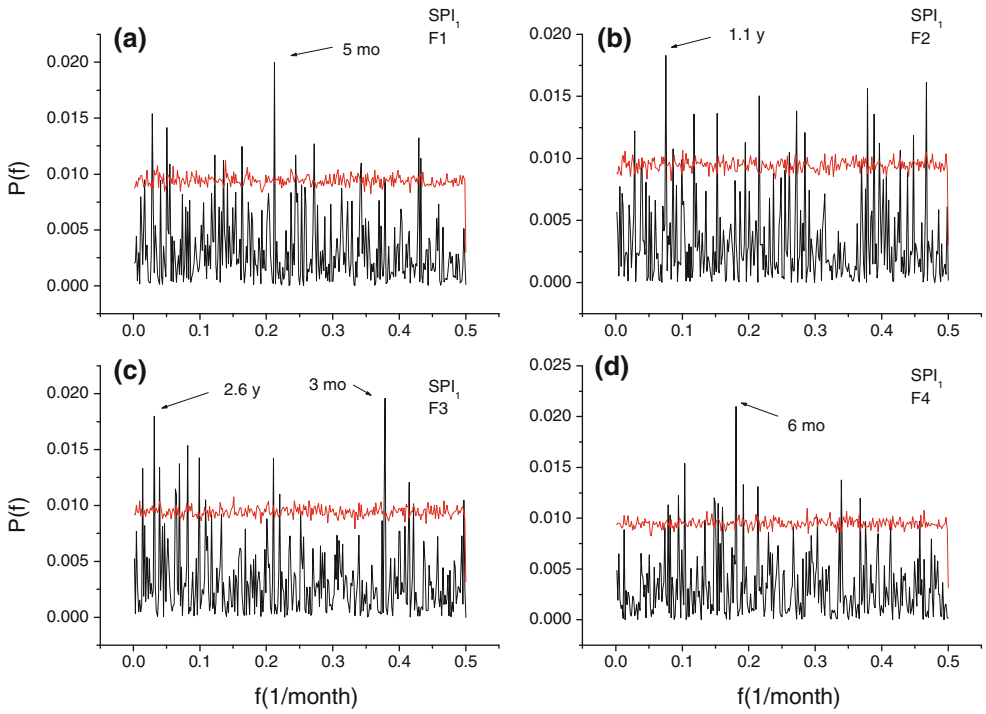

Fig. 11 Power spectral density of the first four PCA component of the SPI_1

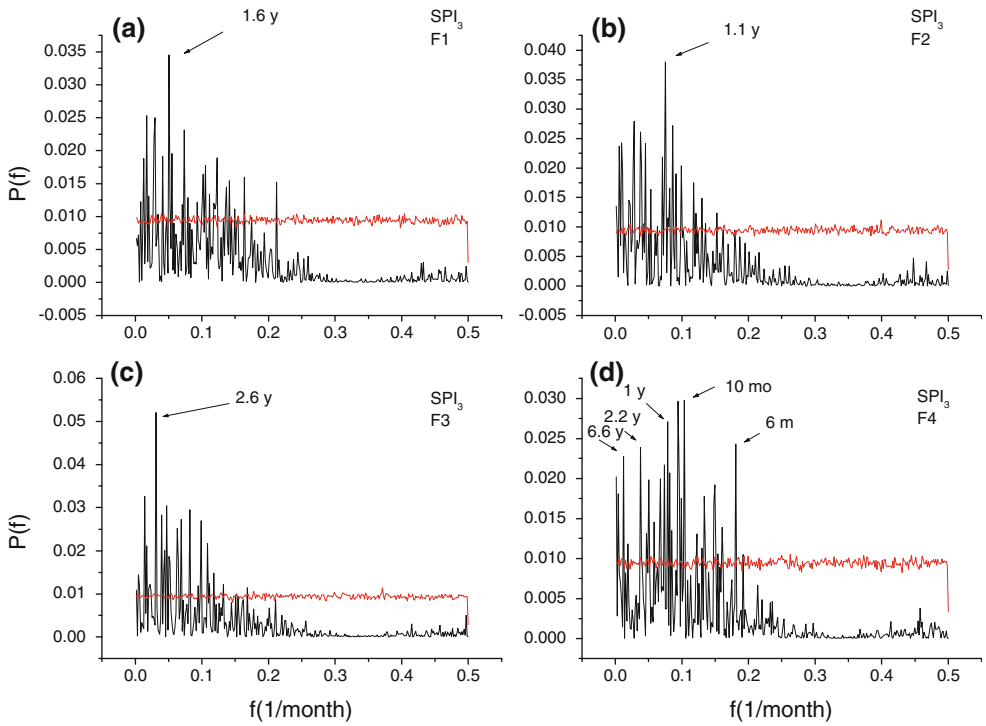

Fig. 12 Power spectral density of the first four PCA components of the SPI_3

precipitation on the selected timescale, as more as increasing the timescale, thus augmenting the long-range correlation of the series. The method of calculating the SPI is equivalent to a white noise filtering, which removes the white noise component of the SPI at the higher frequencies producing such scaling effect; the amount of the white noise component removed increases with the increase of the timescale.

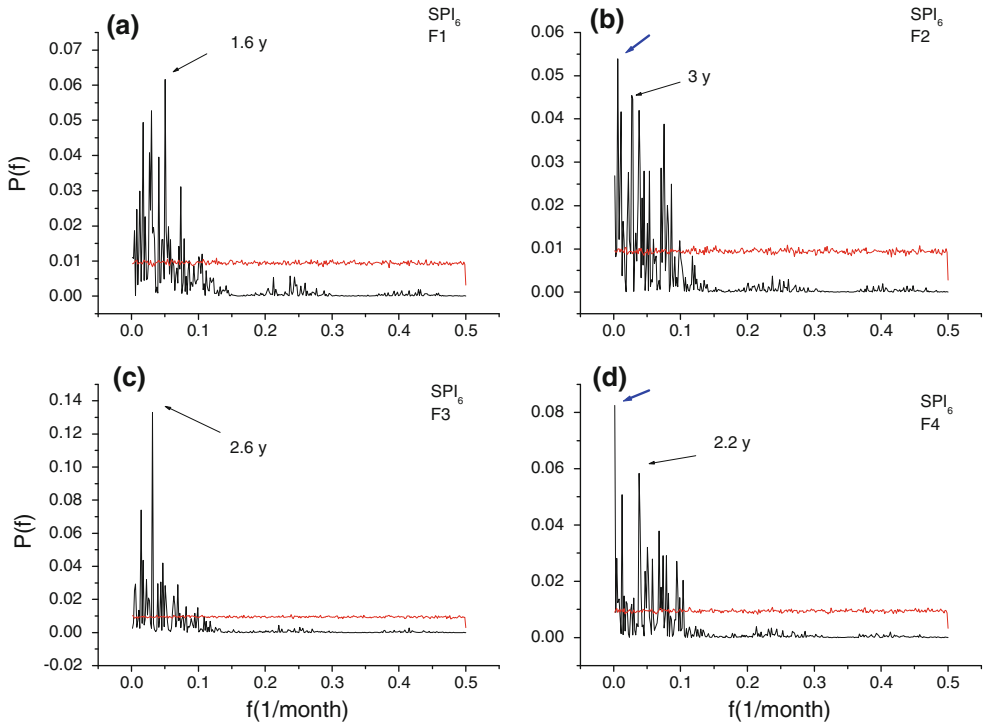

Fig. 13 Power spectral density of the first four PCA components of the SPI_6

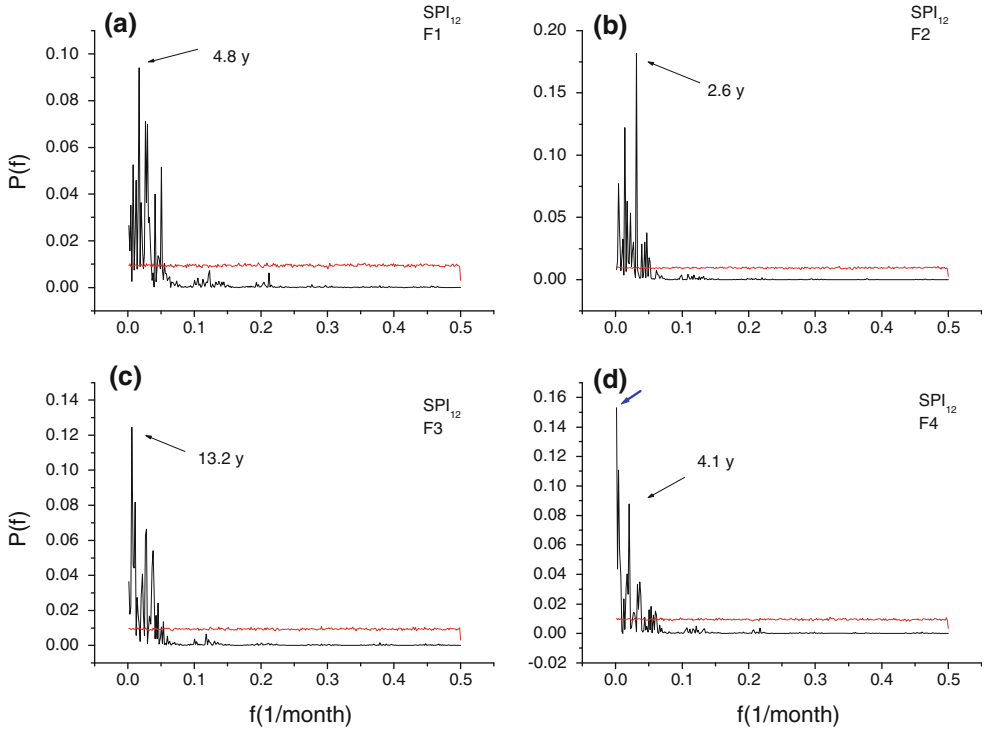

Fig. 14 Power spectral density of the first four PCA components of the SPI_{12}

(iii) *Main frequencies*. The typical significant frequencies of the periodical signals detected in the SPI and SPEI time variability range between intra-annual (6–8 months) to inter-annual (4–5 years) order of magnitude for the lower timescales, while range from intra-annual (3–4 years) to inter-decadal (17–18 years)

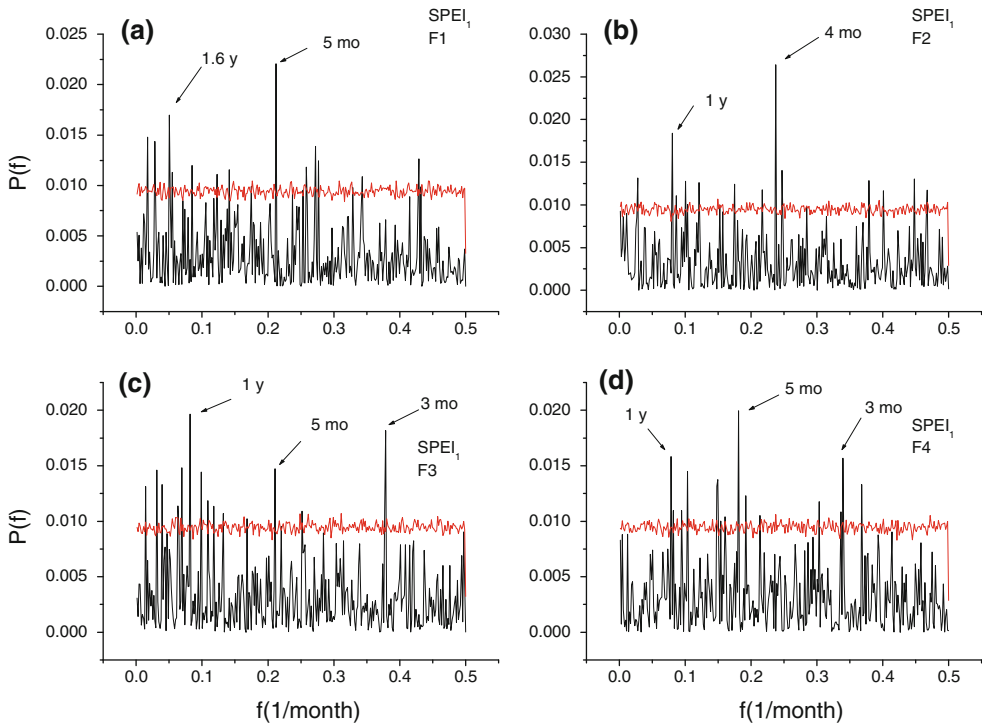

Fig. 15 Power spectral density of the first four PCA components of the $SPEI_1$

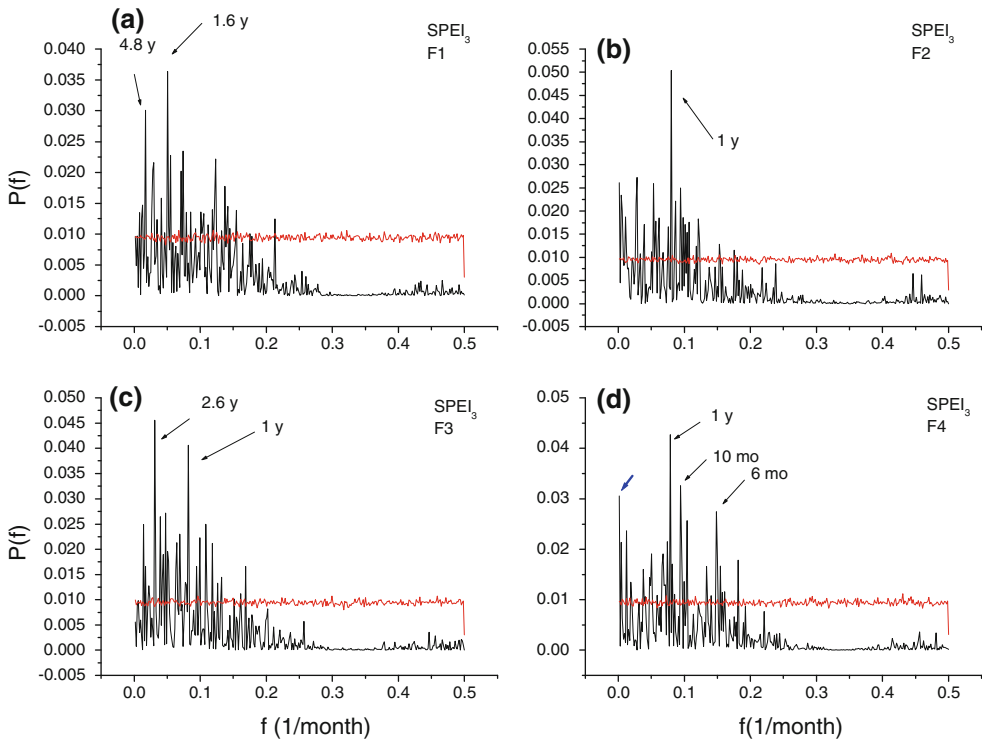

Fig. 16 Power spectral density of the first four PCA components of the $SPEI_3$

order of magnitude for the higher timescales. The knowledge of the typical significant frequencies of the main oscillations governing the index time series can be useful for the long-range predictability of dry and wet periods in the Ebro basin. Bordi et al. (2004) have analysed the spatio-temporal variability of dry and wet

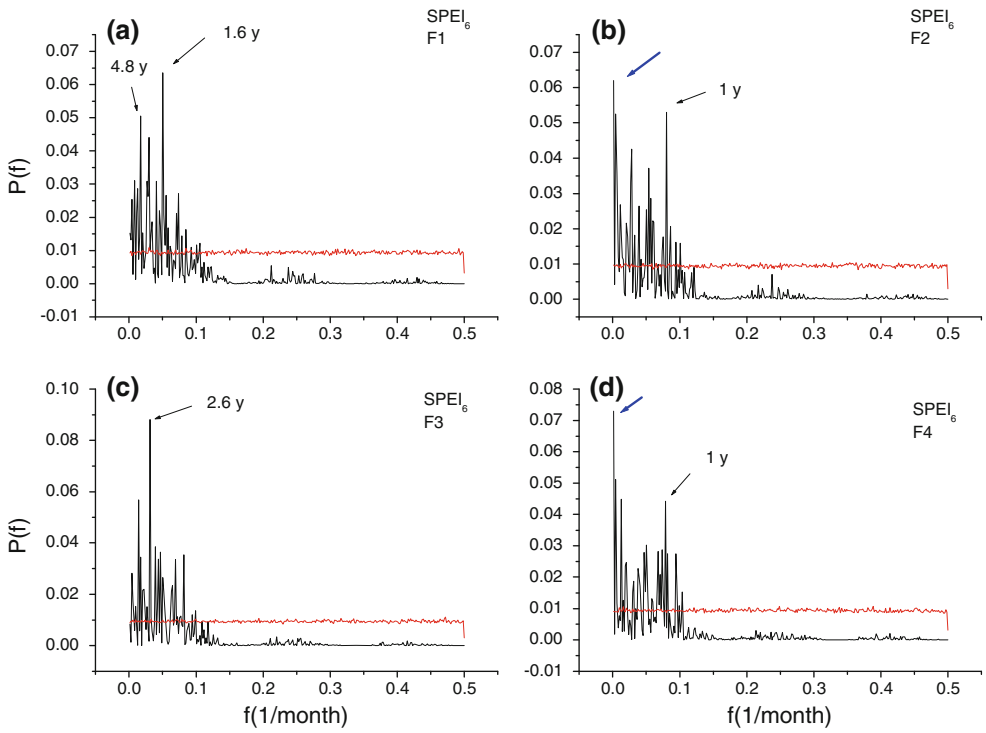

Fig. 17 Power spectral density of the first four PCA components of the $SPEI_6$

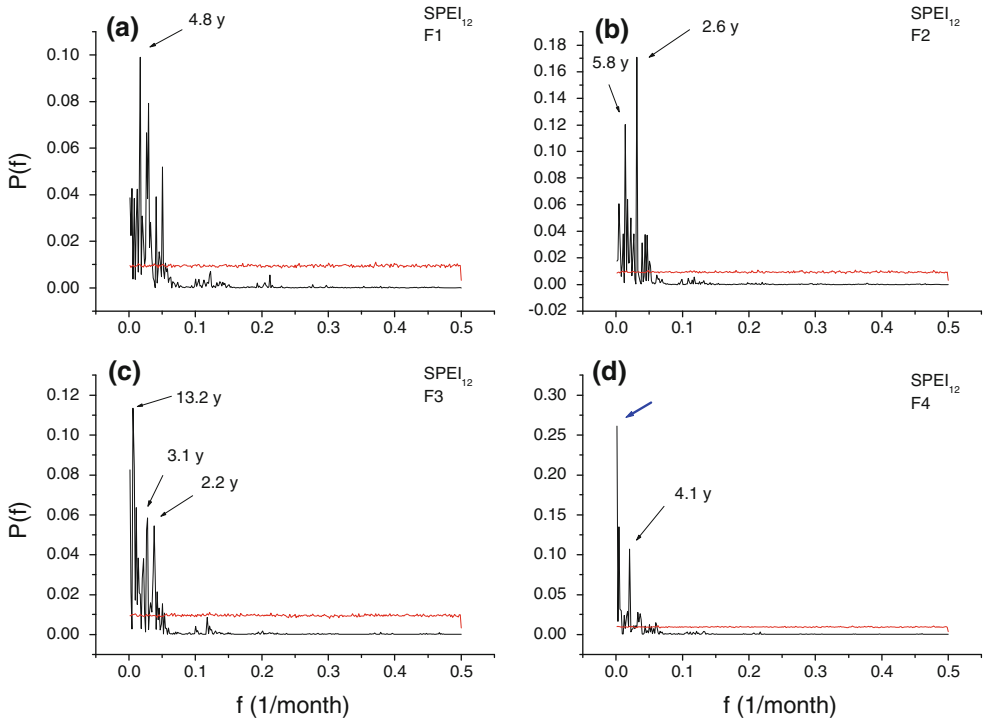

Fig. 18 Power spectral density of the first four PCA components of the $SPEI_{12}$

periods in eastern China and found that SPI_{24} signal is characterized by long-term fluctuations, which contributed to the power spectrum variance at periods varying between 24–16 years (inter-decadal) and 4–3.7 years (inter-annual). Our findings confirm such results. Furthermore, the spectral analysis of the first four principal components of $SPI_{1,3,6,12}$ and $SPEI_{1,3,6,12}$ obtained by using the PCA corroborates such findings (Figs. 11, 12,

13, 14, 15, 16, 17, 18): at timescales of 1 and 3 months intra-annual periodicities are predominant; at timescales of 6 months inter-annual cycles are more evident, and at timescales of 12 moths also inter-decadal periodicities appear. In particular the inter-annual frequency band 3–5 years could suggest a possible link with the El Niño/Southern Oscillation (ENSO) phenomenon (Bordi et al. 2004). A further explanation of such frequency band could be the significant influence of the North Atlantic Oscillation (NAO) on the precipitation regimes in the Mediterranean (Lopez-Moreno and García-Ruiz 2007; Lopez-Moreno and Vicente-Serrano 2008). In fact, it was found by Küçük et al. (2009) that the significant cycle periods at 2–4 years and 6–10 years are evident in the power spectrum of the NAO index. The presence of periodicities with period higher than 10 years could be due to some regional phenomena involving the soil moisture oscillation (Santos et al. 2010, and references therein)

(iv) *Global versus local effect*. The comparative analysis of the spectral properties of the drought indices for all the 45 sites in the Ebro basin lead to the identification of global or regional effects discriminated by local effects: it was found that some periodical signals are common to almost all the sites, while others to only some sites. This finding could lead to recognizing the periodicities that are common to almost all the sites as fingerprints of global or regional phenomena affecting the whole watershed; on the other side, the periodical signals detectable only in a small number of sites could explain some local effects. This discrimination is very clear at timescale of 12 and 24 months (Fig. 9d, f, h, l), in which approximately only one tenth of the 45 sites are characterized by significant frequencies ranging from 8 months to 1.4 years, while the inter-annual and inter-decadal periodicities characterize almost all the sites.

(v) There is a very high climatic contrast as a consequence of the transition between Mediterranean and Atlantic climatic conditions existing in the study area. The intensity of the climatic gradients is a consequence of the short distance between both water bodies and the complex topography which affects the influence of the different air masses even at very short distances (Vicente-Serrano and López-Moreno 2006).

7 Conclusions

This study represents a deep spectral analysis of two drought indices, SPI and SPEI, calculated for 45 meteorological stations in the Ebro basin (Spain) from 1950 to 2006 with timescales varying between 1 and 48 months. Our results point out to a structural similarity between SPI and SPEI, both showing white noise dynamics at the shorter time scales, while appearing persistent at longer time scales. The comparative analysis of the main frequencies detected for both indices in the Ebro basin lead to the identification of global or regional effects (periodical signals are common to almost all the sites) versus local effects (periodical signals characteristic of only few sites). The performed study contributes to a better description and understanding of the hydrological processes governing the Ebro dynamics watershed.

Acknowledgments This work was supported by research projects CGL2011-27536/HID: "Hidrologia nival en el Pirineo central español: variabilidad espacial, importancia hidrológica y su respuesta a la variabilidad y cambio climático", financed by the Spanish Commission of Science and Technology, and FEDER; and ACQWA (FP7-ENV-2008-1-212250). L. Telesca acknowledges the financial support of Gobierno de Aragón (Resolución de 4 de agosto de 2010 del Director General de Investigación, Innovación y Desarrollo, del Departamento de Ciencia, Tecnología y Universidad) and the National Research Council.

References

Abramowitz M, Stegun IA (1965) Handbook of mathematical functions. Dover Publications, New York

Bari Abarghouei H, Asadi Zarch MA, Dastorani MT, Kousari MR, Safari Zarch M (2011) The survey of climatic drought trend in Iran. Stoch Env Res Risk Assess 25(6):851–863

Bordi I, Fraedrich K, Jiang J-M, Sutera A (2004) Spatio-temporal variabilità of dry and wet periods in eastern China. Theor Appl Climatol. doi:10:1007/s00704-004-0053-8

Colombaroli D, Marchetto A, Tinner W(2007) Long-term interactions between Mediterranean climate, vegetation and fire regime at Lago di Massaciuccoli (Tuscany, Italy). J Ecol 95:755–770

Du J, Fang J, Xu W, Shi P (2012) Analysis of dry/wet conditions using the standardized precipitation index and its potential usefulness for drought/flood monitoring in Hunan Province, China. Stoch Environ Res Risk Assess 1–11. doi:10.1007/s00477-012-0589-6

Edwards DC, McKee TB (1997) Characteristics of 20th century drought in the United States at multiple time scales, Atmospheric Science Paper No. 634

El Kenawy A, López-Moreno JI, Stepanek P, Vicente-Serrano SM (in press) An assessment of the role of homogenization protocols in the performance of daily temperature series and trends: application to Northeastern Spain. Int J Climatol. doi:10.1002/JOC.3410

Guttman NB (1998) Comparing the Palmer drought index and the Standardized Precipitation Index. J Am Water Resour Assoc 34:113–121

Guttman NB (1999) Accepting the standardized precipitation index: a calculation algorithm. J Am Water Resour Assoc 35:311–322

Hayes M, Svoboda M, Wall N, Widhalm M (2011) The Lincoln declaration on drought indices: universal meteorological drought index recommended. Bull Am Meteorol Soc 92:485–488. doi:10.1175/2010BAMS3103.1

Heim RR (2002) A review of twentieth-century drought indices used in the United States. Bull Am Meteorol Soc 83:1149–1165

Hosking JRM (1990) L-moments: analysis and estimation of distributions using linear combinations of order statistics. J R Stat Soc B 52:105–124

Iglesias E, Garrido A, Gomez-Ramos A (2003) Evaluation of drought management in irrigated areas. Agric Econ 29:211–229

Jolliffe IT (1990) Principal component analysis: a beginner's guide—I. Introduction and application. Weather 45:375–382

Keyantash J, Dracup J (2002) The quantification of drought: an evaluation of drought indices. Bull Am Meteorol Soc 83:1167–1180

Küçük M, Kahya E, Cengiz TM, Karaca M (2009) North Atlantic Oscillation influences on Turkish lake levels. Hydrol Process 23:893–906. doi:10.1002/hyp7225

Lana X, Serra C, Burgueño A (2001) Patterns of monthly rainfall shortage and excess in terms of the Standardied Precipitation Index for Catalonia (NE Spain). Int J Climatol 21(15):1669–1691

Lázaro R, Rodrigo FS, Gutiérrez L, Domingo F, Puigdefábregas J (2001) Analysis of a 30-year rainfall record (1967–1997) in semi-arid SE spain for implications on vegetation. J Arid Environ 48:373–395

Lloyd-Hughes By, Saunders MA (2002) A drought climatology for Europe. Int J Climatol 22:1571–1592

López-Moreno JI, García-Ruiz JM (2007) Hydrological effects of reservoirs in the Central Spanish Pyrenees. In: Robinson P, Jones JAA, Woo M-K (eds) 2007: managing water resources in a changing physical and social environment. IGU Home of Geography Publication Series, Società Geografica Italiana, Rome, pp 103–114, 177 pp

López-Moreno JI, Vicente-Serrano SM (2008) Positive and negative phases of the wintertime north Atlantic oscillation and drought occurrence over Europe: a multi-temporal- scale approach. J Clim 21:1220–1243

López-Moreno JI, Vicente-Serrano SM, Moran-Tejeda E, Zabalza J, Lorenzo-Lacruz J, García-Ruiz JM (2011) Impact of climate evolution and land use changes on water yield in the Ebro basin. Hydrol Earth Syst Sci 15:311–322

Lorenzo-Lacruz J, Vicente-Serrano SM, López-Moreno JI, Beguería S, García-Ruiz JM, Cuadrat JM (2010) The impact of droughts and water management on various hydrological systems in the headwaters of the Tagus River (central Spain). J Hydrol 386:13–26

McKee TBN, Doesken J, Kleist J (1993) The relationship of drought frecuency and duration to time scales. Eight Conf. On Applied Climatology. Am. Meteor. Soc., Anaheim, CA, pp 179–184

Mishra AK, Singa VP (2010) A review of drought concepts. J Hydrol 391:202–216

Morales A, Olcina J, Rico AM (2000) Diferentes percepciones de la sequía en España: adaptación, catastrofismo e intentos de corrección. Investigaciones Geográficas 23:5–46

Moreira EE, Mexia JT, Pereira LS (2012) Assessing homogeneous regions relative to drought class transitions using an ANOVA-like inference. Application to Alentejo, Portugal Stochastic Environmental Research and Risk Assessment, pp 1–11

Pasho E, Julio Camarero J, de Luis Martín, Vicente-Serrano SM (2011) Impacts of drought at different time scales on forest growth across a wide climatic gradient in north-eastern Spain. Agric For Meteorol 151:1800–1811

Paulo AA, Pereira LS, Matias PG (2003) Analysis of local and regional droughts in southern Portugal using the theory of runs and the standardized precipitation index. In Rossi G, Cancelliere A, Pereira LS, Oweis T, Shatanawi M, Zairi A (eds) Tools for drought mitigation in Mediterranean regions, Kluwer, pp 55–78

Pausas JG (2004) Changes in fire and climate in the eastern Iberian Peninsula (Mediterranean basin). Clim Change 63:337–350

Quiring SM, Ganesh S (2010) Evaluating the utility of the Vegetation Condition Index (VCI) for monitoring meteorological drought in Texas. Agric For Meteorol 150:330–339

Reichstein M, Tenhunen JD, Roupsard O, Ourcival J-M, Rambal S, Miglietta F, Peressotti A, Valentini R (2002) Severe drought effects on ecosystem CO_2 and H_2O fluxes at three Mediterranean evergreen sites: revision of current hypotheses? Glob Change Biol 8:999–1017

Richman MB (1986) Rotation of principal components. J Climatol 6:29–35

Santos JF, Pulido-Calvo I, Portela MM (2010) Spatial and temporal variability of droughts in Portugal. Water Resour Res 46:W03503

Singh VP, Guo FXY (1993) Parameter estimation for 3-parameter log-logistic distribution (LLD3) by Pome. Stoch Hydrol Hydraul 7:163–177

Sivakumar MVK, Motha RP, Wilhite DA, Wood DA (eds) (2010) Agricultural drought indices. Proceedings of an expert meeting, 2–4 June 2010, Murcia, Spain. World Meteorological Organization, Geneva 219 pp

Smith EV (2002) Detecting and evaluation the impact of multidimensionality using item fit statistics and principal component analysis of residuals. J Appl Meas 3:205–231

Telesca L (2010) Analysis of the cross-correlation between seismicity and water level in Koyna area (India). Bull Seismol Soc Am 100:2317–2321

Vicente Serrano SM, López-Moreno JI (2006) The influence of atmospheric circulation at different spatial scales on winter drought variability through a semiarid climatic gradient in north east Spain. Int J Climatol 26:1427–1456

Vicente-Serrano SM (2006a) Spatial and temporal analysis of droughts in the Iberian Peninsula (1910–2000). Hydrol Sci J 51:83–97

Vicente-Serrano SM (2006b) Differences in spatial patterns of drought on different time scales: an analysis of the Iberian Peninsula. Water Resour Manag 20:37–60

Vicente-Serrano SM (2007) Evaluating The impact of drought using remote sensing in a Mediterranean, Semi-Arid Region. Nat Hazar 40:173–208

Vicente-Serrano SM, Cuadrat-Prats JM (2007) Trends in drought intensity and variability in the middle Ebro valley (NE Spain) during the second half of the twentieth century. Theor Appl Climatol 88:247–258

Vicente-Serrano SM, Beguería S, Juan I, López-Moreno MA, García-Vera, Stepanek P (2010a) A complete daily precipitation database for North-East Spain: reconstruction, quality control and homogeneity. Int J Climatol 30:1146–1163

Vicente-Serrano SM, Beguería S, López-Moreno JI (2010b) A multiscalar drought index sensitive to global warming: the standardized precipitation evapotranspiration index SPEI. J Clim 23: 1696–1718

Vicente-Serrano SM, Beguería S, López-Moreno JI (2011) Comment on "Characteristics and trends in various forms of the Palmer Drought Severity Index (PDSI) during 1900–2008" by A. Dai. J Geophys Res-Atmos 116:D19112. doi:10.1029/2011JD016410

Wilhite DA (1993) Drought assessment, management and planning: theory and case studies. Kluwer, Boston

Wu H, Hayes MJ, Wilhite DA, Svoboda MD (2005) The effect of the length of record on the standardized precipitation index calculation. Int J Climatol 25:505–520